ACS OMEGA

Open Access

http://pubs.acs.org/journal/acsodf

Article

Shale Matrix Petrophysical Evolution due to Spontaneous Water Imbibition

Yingying Xu,* Hai Li, Zhiming Hu, Xiangui Liu, Xianggang Duan, and Jin Chang

Cite This: *ACS Omega* 2023, 8, 46746−46756

Read Online

ACCESS | Metrics & More | Article Recommendations

ABSTRACT: Shale matrix alteration resulting from fracturing water−rock interactions has become a major concern. It significantly affects economic production from shale gas formation. Previous studies mostly failed to investigate the thickness of the water intrusion zone and quantified its effects on shale geophysical alteration. As a result, we present a one-dimensional counter-current water imbibition model in which capillary pressure and chemical osmosis stress are included. This model is used to predict water front movement with respect to soaking durations. Based on the simulation results and theory derivations, the matrix porosity-permeability and mechanical alteration models are set up to reveal shale geophysical variables change due to shale−water interactions. Our results show that during the water imbibition process, capillary pressure plays a more crucial role than osmosis pressure. Furthermore, both core-scaled porosity and permeability are negatively associated with water saturation, the extent of which depends on different driving forces and penetration depth. Finally, water soaking is quantitatively demonstrated to induce an increase in compressive strength and stress sensitivity but a reduction in the elastic modulus. These findings will provide efficient insights into driving mechanisms involved in the water−rock interactions. The study is useful to be incorporated into production models for predicting hydrocarbon production from shale reservoirs.

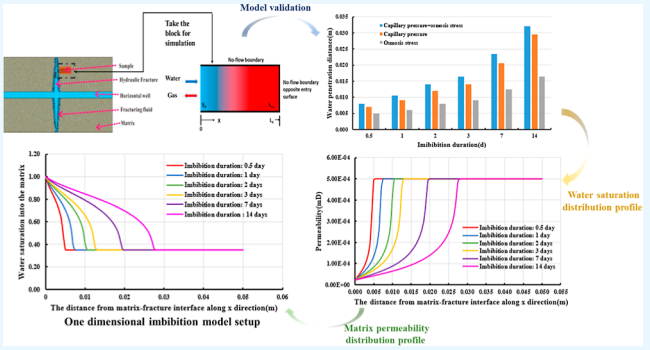

1. INTRODUCTION

Hydraulic fracturing is an important technique for liberating hydrocarbons from unconventional reservoirs, by pumping water-based fluids into the formation to promote economic production.[1] However, it is demonstrated that the recovery rate of the flowback water in unconventional systems is always less than 30%.[2−5] It is largely attributed to water spontaneous imbibition into the formations. In addition, spontaneous imbibition is of particular importance to hydrocarbon recovery during the flowback period. It is referred to as the process of a porous rock absorbing a wetting phase without any external force to displace a nonwetting phase inside porous media.[6] Furthermore, spontaneous imbibition can exist as two typical modes: counter-current and cocurrent.[7−9] For counter-current spontaneous imbibition, the wetting phase will drain the nonwetting phase by the flow in the opposite direction of cores. By contrast, cocurrent spontaneous imbibition is defined as the same flow direction for two phases through both open ends of porous rock.

There are several common imbibition mechanisms that drive liquid into a deeper matrix. Laboratory works have been performed to identify that the spontaneous imbibition in shales is highly correlated with the capillary pressure due to the extremely fine pore sizes.[10−13] Capillary force has been defined as the differential pressure of nonwetting phase and wetting phase across the interface of two immiscible fluids.[14] The high capillary pressure of partially saturated shale matrix makes it possible for a considerable amount of fracturing water infiltration into the rock matrix.[15] In addition to capillary pressure, clay water absorption and chemical osmosis have been investigated to be additional driving forces for water imbibition of shale systems.[16−19] Osmosis pressure mostly originates from a semipermeable membrane separating two aqueous solutions of different chemical potential due to a salt concentration difference. It only allows water molecules or uncharged molecules to move through by forming a diffusive double layer.[20] Clay minerals can function as a semipermeable membrane because of the negative charges on clay particle surfaces.[21,22] The negative charges attract cations in solution to adsorb onto the clay surface and form the double layer. The osmotic pressure in clay-rich sediments leads water molecules to transport from the low-salinity fluids to the high-salinity

Received: August 17, 2023
Revised: November 18, 2023
Accepted: November 22, 2023
Published: December 1, 2023

formation brine until the salt concentration reaches an equilibrium.[23,24] For this reason, the water-sensitive cores (i.e., clay mineral) are observed to expand in volume upon exposure to fresh water.[21]

Water invasion into the shale fracture surface or within the matrix will lead to formation damage. As a result, shale strength and other mechanical properties can be weakened post fracturing operations.[25−27] Thus, induced fractures can be more easily generated. Besides, experimental investigations on shale−water interactions have previously showed the dramatic alteration in permeability and porosity by the generation of fractures,[28−30] particle detachment,[31] and plugging of flow channels,[32] as well as the occlusion of pore spaces,[33−35] thereby impacting hydrocarbon recovery.[36−38]

Although the fracturing water imbibition in shale reservoirs is well recognized both from imbibition models and experimental approaches,[39−42] our insights into the imbibition mechanism mostly focus on capillary pressure, ignoring the impact of chemical osmosis. It can lead to an understanding of inaccuracy in the water imbibition process. Additionally, the above studies were qualitatively performed on the shale petrophysical evolution (i.e., porosity and permeability) from the perspective of water saturation or external water imbibition weight. Thus, we have little quantitative information about the fracturing water penetration distance and water saturation distribution into the matrix. Moreover, the mathematical correlation between matrix permeability and porosity with respect to spontaneous imbibition is rarely known so far.

Thus, the goals of the present study are involved in (1) setting up a one-dimensional water imbibition numerical simulation for the shale matrix to analyze and compare water dynamic saturation profiles and (2) using this model to explore shale matrix permeability and porosity alteration profiles. Moreover, the mathematical correlation between permeability, porosity, and water saturation can be determined; (3) based on this model, analyzing mechanical evolution and matrix stress-dependent permeability for water-sensitive minerals resulted from water−rock interactions. This study offers a mathematical method for characterizing shale spontaneous imbibition and its effect on shale geophysical alteration. The study provides a theoretical understanding for incorporating water uptake into the production prediction model for shale gas exploitation.

2. METHODOLOGY

2.1. Imbibition Mechanisms. A spontaneous imbibition process is mostly determined by an interplay of driving forces, including capillary force and chemical osmosis pressure, respectively.[43,44] Capillaries can last a long time during postfrac production. Later, a new imbibition mechanism as a chemical osmosis is taken into account, which is further incorporated into the proposed water imbibition numerical model in the paper.

2.1.1. Chemical Osmosis. When confronted with aqueous solution differences on the both sides of clay membrane, osmosis will take place to drive the water to the lower concentration side of the membrane into the clay, ultimately leading to clay swelling, governed by eq 1[21]

$$p_\pi = \frac{RT}{\overline{V}_w} \ln \frac{x_1}{x_2} \tag{1}$$

where: p_π is the chemical osmotic pressure, Pa; R is the ideal gas constant, 8.314 J/(mol·K); $\overline{V}_w$ is the partial molar volume of water, 18.02×10^{-6} m^3/mol; T is the temperature, K; and x_i is the water activity of solution i (i = 1, 2), nondimensional.

The concentration difference is introduced into the osmotic pressure, which is also defined as eq 2

$$p_\pi = \nu RT(c_2 - c_1) \tag{2}$$

where: c_i is the concentration of solution i (i = 1, 2) for water activity x_i, mol/m^3 and ν is the constituent number of ions, nondimensional.

However, naturally most of the semipermeable membrane exhibits nonideality and cannot still exclude some charged solutes from the membrane besides water molecules. Thus, the membrane coefficient is used to account for capacity of semipermeable membrane restricting charged particles from passing through, which ranges from 0 (nonmembrane) to 1(ideal membrane).[45] Therefore, osmosis pressure is given by expression 3

$$p_\pi = \lambda \nu RT(c_2 - c_1) \tag{3}$$

where: λ is the membrane efficiency, nondimensional.[46]

2.1.2. Capillary Pressure. According to the Young−Laplace law, capillary force can be calculated as well, given by eq 4, depending on surface tension σ, contact angle θ, and pore throat radius r. r depends on the pore network system and cannot be modified unless geomechanics effect or chemical alteration is considered. However, surface tension and contact angle refer to relative strength of molecular interactions at the rock−fluid interface or fluid−fluid interface.[47]

$$p_c = p_{nw} - p_w = \frac{2\sigma \cos\theta}{Ar} \tag{4}$$

where: P_c is the capillary pressure, Pa; P_{nw} is the hydrostatic pressure of nonwetting phase, Pa; p_w is the hydrostatic pressure of wetting phase, Pa; σ is the surface tension of wetting phase and rock interface, $N.m$; 6 is the contact angle, deg; r is the pore radius, m; and A is the contact surface area, m^2.

In this study, the capillary force and osmotic pressure are attributed to spontaneous imbibition. Hence, the total driving pressure p is written as expression 5

$$p = p_\pi + p_c \tag{5}$$

2.2. Water Imbibition Mathematical Modeling. For shale gas reservoirs with stimulated reservoir volume, the injected fluid invades into a tight matrix under capillary pressure and chemical osmosis, while gas flows reverse into the fracture during liquid injection and soaking. This phenomenon can be simplified as the one-dimensional countercurrent imbibition process, indicating that only one open face can contact the fracturing fluid, as demonstrated in Figure 1. To simplify the solution procedure, the following assumptions are made:[48,49] (1) the imbibition process involves piston-like displacement of the gas−water phase in the matrix system; (2) shale is homogeneous and isotropic, without considerations of bedding effects; (3) the compressibility of the rock skeleton remains constant during the imbibition process; (4) the seepage conforms to Darcy's law in the imbibition process, which is approximately considered to be instantaneously steady; (5) the gravity is so small that it can be ignored in the imbibition simulation model compared to capillary pressure and osmotic pressure.

According to the Darcy's formula, the gas and water flow rates during imbibition are given by eqs 6 and 7, respectively

https://doi.org/10.1021/acsomega.3c06079
ACS Omega 2023, 8, 46746−46756

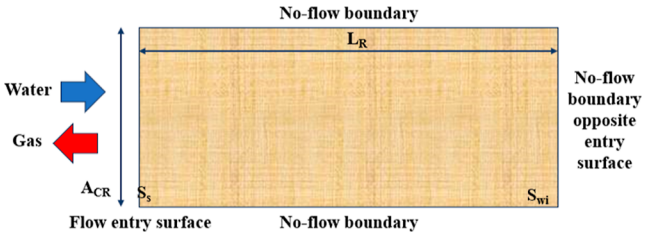

Figure 1. Schematic diagram of 1D counter current imbibition into the matrix process. The left diagram describes hydraulic fracturing spontaneous imbibition. The right diagram depicts that water is imbibing through the open boundary from left to right, expelling the gas phase the opposite way. The initial water saturation is Swi, and maximum water saturation at the inlet is Ss. The length of the rock sample boundary is L_R and the cross-sectional area is A_{CR}.

$$v_g = -\frac{KK_{rg}}{\mu_g}\frac{\partial S_w}{\partial x}\frac{\partial}{\partial S_w}(p + p_w) \tag{6}$$

$$v_w = -\frac{KK_{rw}}{\mu_w}\frac{\partial S_w}{\partial x}\frac{\partial p_w}{\partial S_w} \tag{7}$$

The relative permeability curves for gas and water phases are assumed to follow the Brooks-Corey model,[50] expressed by eqs 8 and 9

$$K_{rg} = K_{rgd}\left(1 - \frac{S_w - S_{gr}}{1 - S_{gr} - S_{wr}}\right)^{n_g} \tag{8}$$

$$K_{rw} = K_{rwd}\left(\frac{S_w - S_{wr}}{1 - S_{gr} - S_{wr}}\right)^{n_w} \tag{9}$$

The matrix capillary pressure for imbibition is modeled with the Brooks−Corey model,[50] written in eq 10

$$p_c = p_{cmax}\ln\frac{S_w - S_{wr}}{1 - S_{wr} - S_{gr}} \tag{10}$$

where v_g and v_w are gas and water flow rates, respectively, m^3/s; K is the absolute permeability, mD; K_{rg} and K_{rw} are the relative permeability of gas and water phases, respectively, nondimensional; μ_g and μ_w are the viscosity of gas and water, respectively, mpa.s; p and p_w are the total driving pressure for imbibition and hydrostatic pressure of water, respectively, Pa; and x is fluid flow distance along the x direction, m; K_{rgd} is the gas end point, nondimensional; K_{rwd} is the water end point, nondimensional; p_{cmax} is the maximum capillary pressure, Pa; S_{gr} is the irreducible gas saturation; S_{wr} is the irreducible water saturation; n_w is the Corey exponent for water; and n_g is the Corey exponent for gas.[51]

The material balance of countercurrent imbibition is given below as 11

$$v_w + v_g = 0 \tag{11}$$

We can substitute 6 and 7 into expression 11 and the flow rate for the water phase is given by 12

$$v_w = D(S_w)\frac{dS_w}{dx} \tag{12}$$

where: $D(S_w) = K\frac{K_{rg}K_{rw}}{K_{rg}\mu_w + K_{rw}\mu_g}\frac{d}{dS_w}(p_c + p_{\pi w})$, defined as effective capillary diffusivity coefficient, m^2/s.

Then the water phase mass conservation equation is given by expression 13

$$\frac{\partial \varphi S_w}{\partial t} = \frac{\partial}{\partial x}\left(D(S_w)\frac{\partial S_w}{\partial x}\right) \tag{13}$$

where φ is the matrix porosity, nondimensional, and t is the imbibition duration, s.

At the initial time, the matrix has the same initial water saturation, and the positions of $x = 0$ and $x = L_R$ are open to external water and a closed surface, respectively. The initial condition and boundary conditions are given as follows:

Initial condition

$$S_w(x, t=0) = S_{wi} \tag{14}$$

Inner boundary condition

$$S_w(x=0,t) = S_s \tag{15}$$

Outlet boundary condition

$$\frac{\partial S_w}{\partial x}|_{x=LR} = 0 \tag{16}$$

2.3. Model Solution. The finite difference method is used to solve water imbibition partial equations with forward difference discretization in time and center difference discretization in space using the Matlab programming language. There are five main steps in the algorithm: (1) the position and time are discretized into $i*n$ grids, and then each saturation in the grid network is introduced. Thus, the previous nonlinear partial differential equations are discretized into linear difference equations; (2) the convergence time step Δt and distance step Δx are determined to make equations finally converged; (3) initial conditions are set; (4) the effective diffusion coefficient term compute at each time step and each position are computed; (5) the discretized water saturation along with boundary conditions and initial conditions at convergence time step are solved, and then the imbibed water volume and imbibition rate can be calculated based on the water saturation profiles.

The discretized differential equations and auxiliary conditions for the water imbibition process are written in eqs 17−22:

For the 2 to i-1 grid of space, the difference equation is

$$\varphi\frac{(S_w)_i^{n+1} - (S_w)_i^n}{\Delta t} = \frac{D_{i+1/2}((S_w)_{i+1}^{n+1} - (S_w)_i^{n+1}) + D_{i-1/2}(-(S_w)_i^{n+1} + (S_w)_{i-1}^{n+1})}{\Delta x^2} \tag{17}$$

where

$$D_{i+1/2} = \frac{D_{i+1} + D_i}{2} \tag{18}$$

$$D_{i-1/2} = \frac{D_{i-1} + D_i}{2} \tag{19}$$

For the first grid of space

$$(S_w)_1^{n+1} = S_w \tag{20}$$

For the first grid of space

$$\frac{(S_w)_i^{n+1} - (S_w)_{i-1}^{n+1}}{\Delta x} = 0 \tag{21}$$

https://doi.org/10.1021/acsomega.3c06079
ACS Omega 2023, 8, 46746−46756

Initial conditions for each space grid

$$(S_w)_i^0 = S_{wi} \tag{22}$$

The water imbibition accumulation is mathematically given by eq 23

$$W = \int_0^L A_c \varphi (S_w - S_{wi}) dx \tag{23}$$

where W is the imbibed water volume, m^3; A_c is the cross section area of the core, m^2; and L is the core length, m.

The water imbibition rate is thus derived from 23, written in eq 24

$$q = \frac{dW}{dt} \tag{24}$$

where q is the water imbibition rate, m^3/s.

2.4. Model Validation. To validate the mathematical model, the hydraulic fracturing and reservoir properties data from onsite gas shale are used for history matching and predicting the water imbibition process. The initial input parameters of the model are summarized in Table 1. The

Table 1. Basic Input Parameters for the Model in This Study

parameters	value	parameters	value
matrix permeability (mD)	5×10^{-4}	water viscosity (mPa•s)	0.001
matrix porosity, dimensionless	0.045	gas viscosity (mPa•s)	0.03
core diameter(m)	0.025	experimental temperature (K)	300
core length(m)	0.05	Kr end point of water Krw	0.1
initial water saturation	0.35	Kr end point of gas Krg	0.65
irreducible water saturation	0.35	equivalent salinity in the matrix (ppm)	5000
irreducible gas saturation	0.3	maximum capillary pressure (KPa)	1100
water corey nw	4	gas corey ng	2
initial core pressure(MPa)	50	outlet core pressure (MPa)	5
initial Young's elastic modulus(GPa)	20		

history data matching results are shown in Figure 2, which resulted in a reasonable fitting between the observed experimental results and calculated imbibition volume versus time.

We used the model to calculate gas−water phase relative permeability alteration caused by water saturation (Figure 3). It is observed in Figure 3 that a relatively small increase in water saturation from the initial value can account for a sharp decline in gas relative permeability followed by a plateau of permeability close to zero. In contrast with the gas phase, the initially immobilized water is able to flow until the water saturation reaches about 0.5. Thereafter, the relative permeability for the water phase will enhance greatly at each water saturation increment. The water relative permeability can get the maximum value when imbibition ends at a saturation of 0.65.

In addition, we modeled the driving force evolution with respect to matrix water saturation, ad presented in Figure 4. The osmotic pressure induces fluid transport from low-salinity to high-salinity through a clay membrane to eliminate chemical potential caused by a salinity difference. Thus, chemical

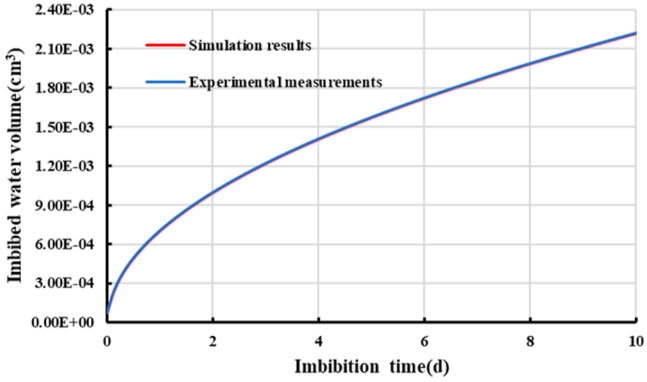

Figure 2. Fitting comparison between simulation results and experimental observation.

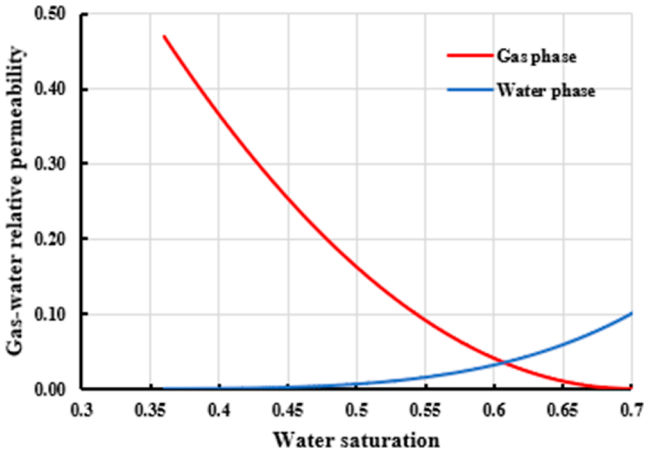

Figure 3. Gas−water relative permeability curve.

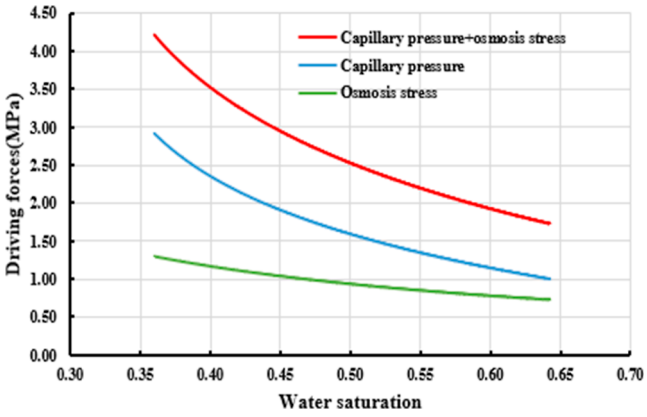

Figure 4. Comparison between driving forces versus core water saturation.

osmosis will decrease as water is gradually driven into a high-salinity matrix to reduce the salinity. Likewise, the capillary pressure is linearly associated with a net effect of gas and water phase hydraulic pressure by definition. This pressure can result in the wetting phase (water) imbibed into rocks and will diminish with increasing water saturation. This phenomenon can be attributed to increased water wettability caused by water−rock interactions, which will decrease the capillary pressure gradient. It is clearly noticed that the capillary pressure curve is still higher than chemical osmosis when water saturation changes.

https://doi.org/10.1021/acsomega.3c06079
ACS Omega 2023, 8, 46746−46756

Moreover, we compared the imbibition process driven by different driving forces. The simulation results revealed in Figures 5 and 6 that the imbibition rate and water imbibition

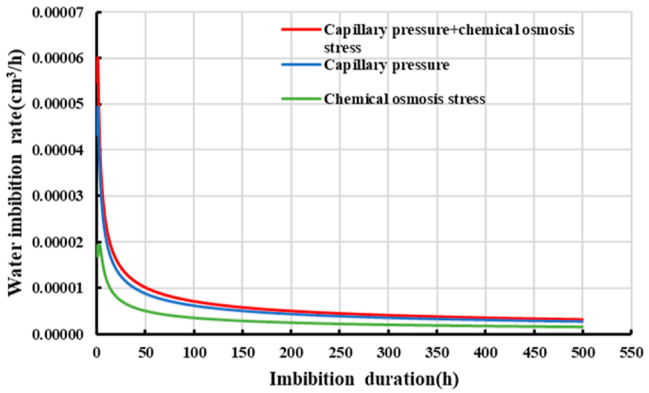

Figure 5. Relation between the water imbibition rate and imbibition duration.

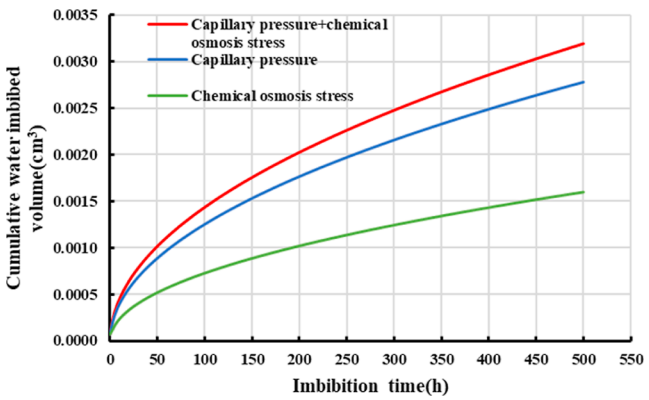

Figure 6. Relation between water imbibition volume and imbibition duration.

accumulation depend largely on the internal impetus mechanisms. The curve trend in Figure 5 illustrated that there is an enhancement in imbibed water volume with the increase in imbibition duration. Generally, at the early stage of water imbibition curves, the amount of water imbibed increases rapidly. However, at the later stage, the amount of water imbibed increases slowly until it no longer changes.

It is calculated in Figure 6 that under the comprehensive driving forces, the water imbibed volume is apparently 20 and 100% higher than that resulted from capillary forces and osmosis stress, respectively, at duration of 500 h, namely, about 21 d. It indicated that capillary forces play a vital role in the imbibition process. As a result, we can get the biggest decline in the initial water imbibition rate controlled by osmosis, then it comes to second by capillary forces, whereas it takes much more time for the water imbibition rate to drop by the capillary and osmosis pressure interplay.

3. RESULTS AND DISCUSSION

3.1. Water Saturation Profiles. The water saturation distribution at different distances along the imbibition direction with respect to various imbibition durations is obtained in Figure 7, 8, and 9, respectively. These figures depict a water movement front profile. As is shown in these figures, at a fixed time, the water saturation decreases gradually

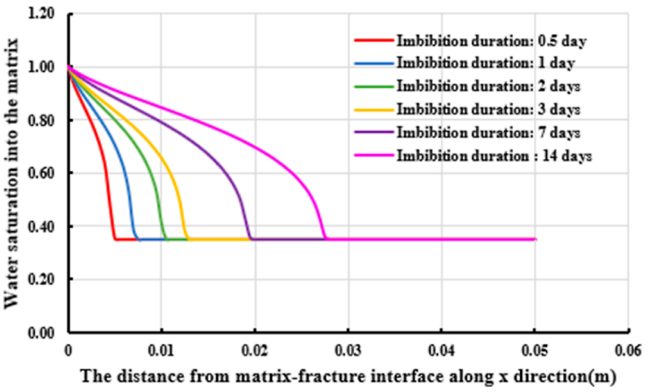

Figure 7. Water saturation profiles into the shale matrix resulted from chemical osmosis and capillary pressure.

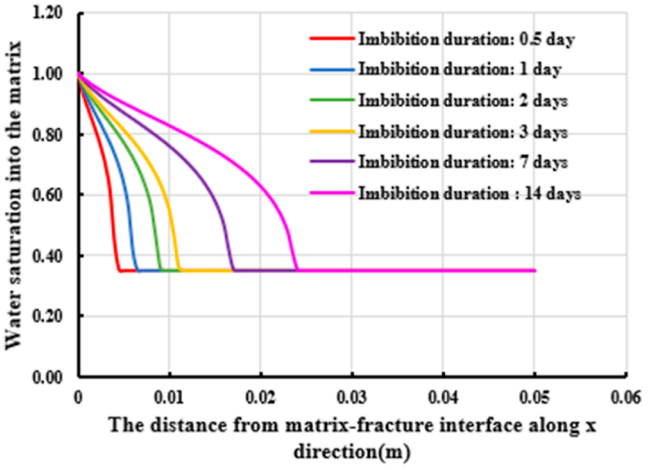

Figure 8. Water saturation profiles in the shale matrix resulted from capillary pressure.

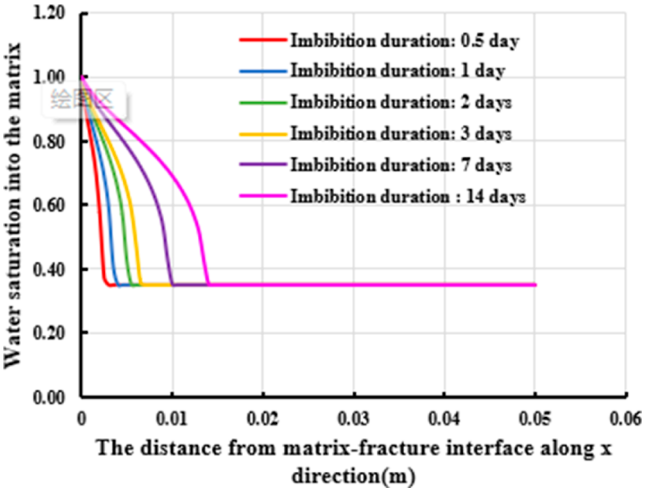

Figure 9. Water saturation profiles into the shale matrix resulted from chemical osmosis pressure.

with the increase in the penetration distance. At a fixed position, the water saturation increases with increasing imbibition time. For a certain position and time during the imbibition process, we can obtain the value of the water saturation.

https://doi.org/10.1021/acsomega.3c06079
ACS Omega 2023, 8, 46746−46756

It is observed as well from Figure 10 that we can determine the water penetration depth into the matrix. The position $x = 0$

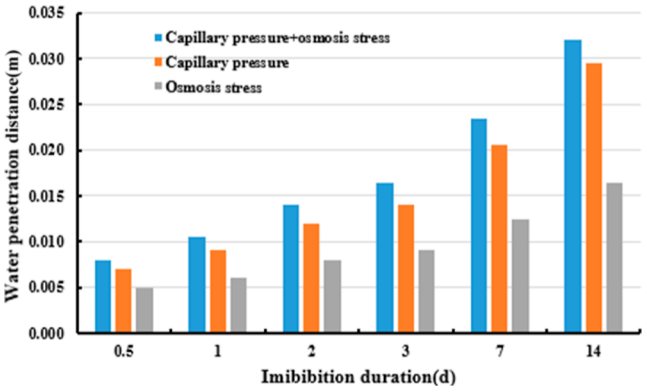

Figure 10. Water penetration distance versus imbibition duration curve.

is assumed as a matrix−fracture interface, filled with a water of $S_w = 1$. The water uptake penetration depth in 1 day reaches about 5 mm and water wetting front has moved more than 0.30 cm forward after 14 days, which is in good agreement with the assumption of a semi-infinite porous medium and agrees with the study of literature (51). This depth range is mostly due to the inherently low permeability and porosity of shale. Furthermore, the imbibition distance of water front into the matrix is proven to be the highest among three geophysical conditions. It is because more external forces exerted on the water phase can drive it more further into the rock and cause a much bigger altered zone of the matrix. The penetration distance controlled by capillary pressure can be close to 0.30 cm while the length in the matrix-altered zone only driven by chemical osmosis stress can be just over 0.015 cm after 14 days.

For each moment during the imbibition process, we can calculate the average water saturation simply by integrated water saturation at each position point. The mathematical equation is given by expression 25

$$S_{wa} = \frac{\int_0^L S_w(x, t)\mathrm{d}x}{L} \tag{25}$$

where S_{wa} is the water average saturation in the core, dimensionless.

As shown in Figure 11, we observed that the water saturation at the core scale is positively correlated with imbibition duration driven by different mechanisms. Apparently, the most significant increase in water saturation from an initial value of 0.36 to water saturation of 0.65 after a 500 h-imbibition process predominated by total driving forces. However, the water saturation curve inclines most slightly during the same soaking time, altering from 0.36 to less than 0.5 as a result of osmosis stress.

3.2. Porosity Alteration. Under the control of multiple driving forces, water will intrude into the matrix pores and then occupy the micropores by forming water adsorption films and inducing clay swelling, leading to a reduction in matrix porosity.

The absorbed water volume is given by eq 26[52]

$$V_w = \beta p_s^{D-3} x_c V \tag{26}$$

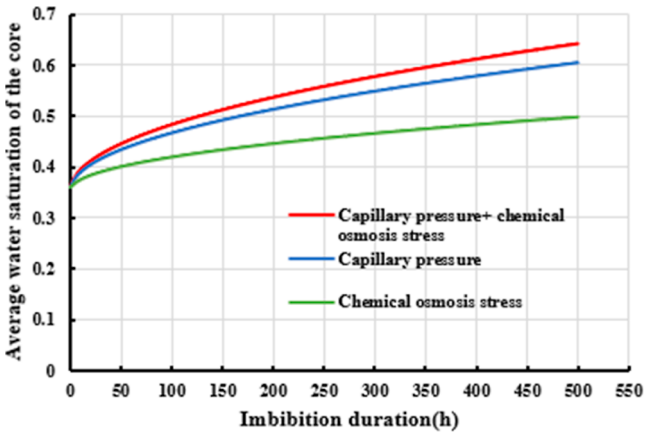

Figure 11. Core average water saturation with respect to the imbibition duration curve.

where: V_w is the absorbed water volume, m^3; β is the swelling coefficient, depending on the temperature and clay properties; D is the surface fractal dimension of clay minerals, closely related with irregularities and surface roughness of clay; x_c is the clay volume percent in the core, dimensionless; V is the rock apparent volume, m^3; and p_s is the effective pressure, Pa.

Considering the swelling stress derived from osmosis, the effective pressure exerted on swelling rock is calculated as eq 27 based on a fractal theory[52]

$$p_s = p + p_{swell} \tag{27}$$

where: P is the overburden pressure and Pa; p_{swell} is the swelling pressure, Pa.

The swelling pressure is given by eq 28[52]

$$p_{swell} = p_\pi \left(\frac{p}{p_\pi}\right)^{D-2} \tag{28}$$

The effect of clay swelling varies with position and time due to varying water saturation, leading to different porosities with duration. As a result, the porosity profile after clay swelling can be mathematically obtained as expression 29

$$\varphi_e = \varphi - \beta p_s^{D-3} x_c \tag{29}$$

where φ_e is matrix porosity at each point and time after clay swelling, dimensionless.

Moreover, combining eq 29, the effective porosity can further be written at the core-scale, taking the form of eq 30

$$\varphi_a = \frac{\int_0^L \varphi_e \mathrm{d}x}{L} \tag{30}$$

where φ_a is the effective matrix porosity at the core-scale, dimensionless.

Model simulation lasting for 14 days shows that water imbibition resulting from different driving forces can cause distinctions in penetration depths, leading to further porosity evolution (Figure 12, 13, and 14). The porosity increases from the lowest value at the matrix−fracture interface to the original value with the increase in the penetration distance. The pores and flow paths are closer to the interface, the more likely the flow path can be saturated with water. Therefore, it is more possible for water to clog the pores into the matrix, leading to lower porosity. Meanwhile, the porosity decrease is predicted

https://doi.org/10.1021/acsomega.3c06079
ACS Omega 2023, 8, 46746−46756

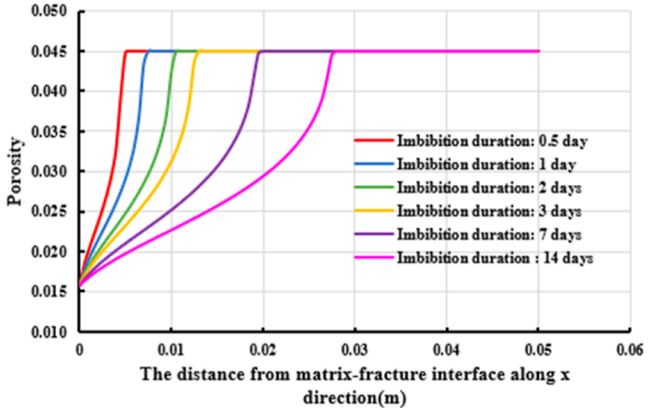

Figure 12. Porosity profile at different imbibition durations driven by the capillary pressure and chemical osmosis force.

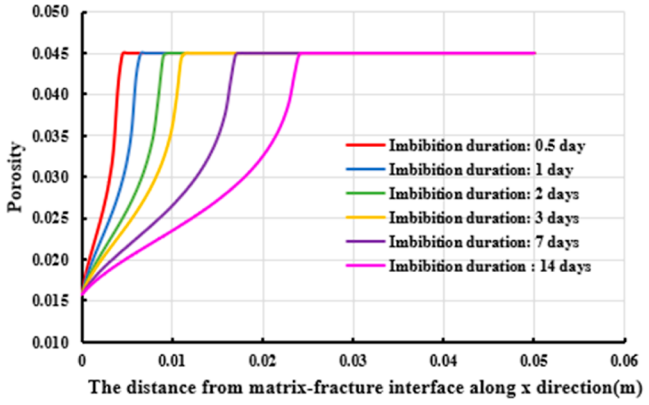

Figure 13. Porosity profile at different imbibition durations driven by capillary pressure.

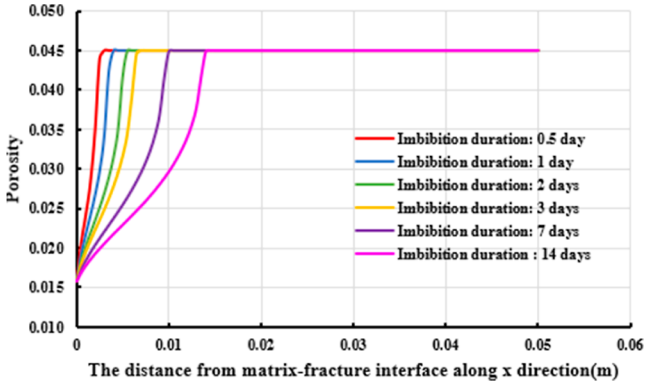

Figure 14. Porosity profile at different imbibition durations driven by the chemical osmosis force.

to be much more noticeable after 14 days than after 3 days of imbibition process. With an imbibition time of 14 days, the core develops the thickest water-altered zone by total forces in Figure 12 but the thickness of altered zone in the core is observed to be the lowest in Figure 14.

Figure 15 shows that calculated porosity for the core, given by eq 30, declines linearly with the increase in the water saturation due to the total driving forces, which is in good agreement with the previous findings in Figures 12−14. Because the imbibed water will occupy the main pores and flow paths due to the generated water film on the inner face of

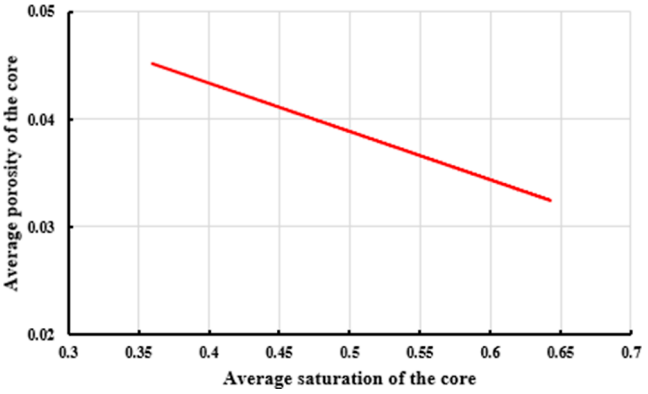

Figure 15. Effective porosity vs average saturation curve at the core-scale.

pores and clay expansion caused by water-sensitive minerals, the porosity will decrease with respect to water saturation.

3.3. Permeability Alteration. According to the Kozeny−Carman equation,[53] involved in the mathematical relationship between porosity and permeability, the matrix permeability can be calculated as expressions 31 and 32

$$K_e = K\left(\frac{\varphi_e}{\varphi}\right)^3 \tag{31}$$

$$K_a = K\left(\frac{\varphi_a}{\varphi}\right)^3 \tag{32}$$

where K_e is the permeability at each point and time inside the matrix, mD and K_a is the effective matrix permeability at the core-scale, mD.

It is seen from Figure 16, 17, and 18 that the permeability increases significantly from the minimum value to initial

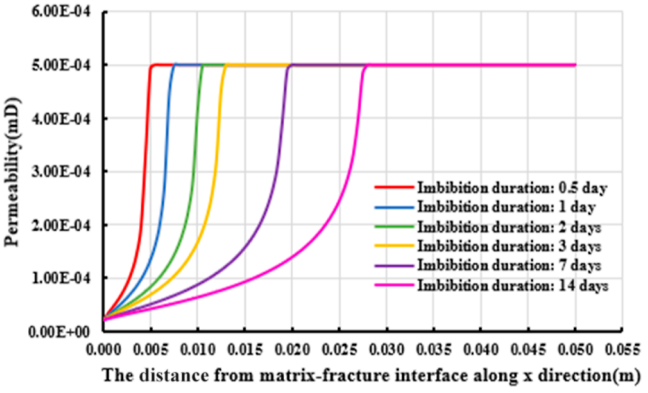

Figure 16. Relation between core permeability and penetration distance into the matrix curve driven by the capillary pressure and chemical force.

intrinsic permeability along the water invasion direction, generating a water alter zone different from the unchanged core. As a result, the altered zone of core has a relatively lower permeability than original core permeability. The permeability has enhanced greatly at the early stage but increased slightly at the later stage, which may depend upon the different distance and driving forces. We can clearly see that the higher driving forces, the farther distance water invades at the same time conditions. The incline in permeability change is still higher

https://doi.org/10.1021/acsomega.3c06079
ACS Omega 2023, 8, 46746−46756

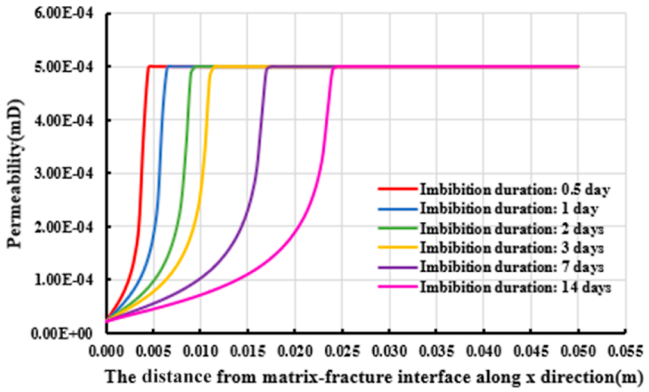

Figure 17. Relation between core permeability and penetration distance into the matrix curve driven by capillary pressure.

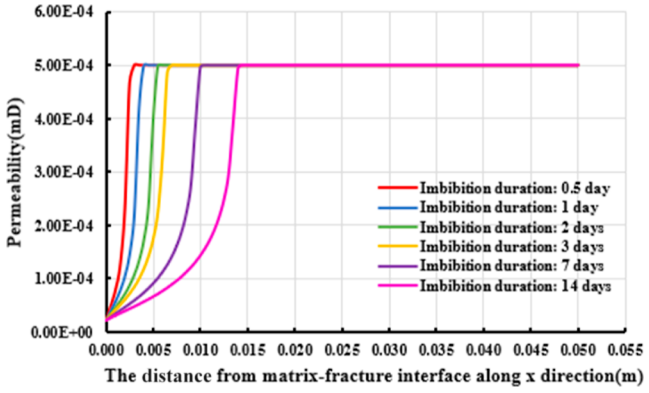

Figure 18. Relation between core permeability and penetration distance into the matrix curve driven by a chemical force.

driven by total forces than that controlled by other forces. These conclusions can provide important insights into predicting the alteration in equivalent permeability and clarifying permeability profiles of altered zone and cores during different shut-in periods.

It is seen from Figure 19 that according to eq 32, calculated permeability for the core has the trend of declination with the increase in the water saturation due to the total driving forces, corresponding to the previous finding in Figures 16−19. This condition is mostly attributed to the occlusion by absorbed water molecules on the inner pore surfaces and clay expansion

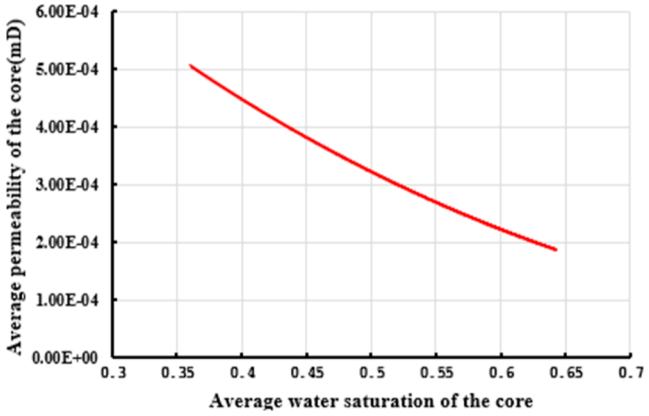

Figure 19. Effective permeability versus average saturation curve at the core-scale.

from water-sensitive minerals, which impact the gas extraction from the matrix to fracture systems and overall hydrocarbon recovery.

3.4. Pressure-Dependent Permeability Alteration.

3.4.1. Elastic Modulus Model of Gas Shale. In this study, damage variable F was introduced to characterize shale damage resulting from the shale−water interaction, defined as the ratio of altered zone area (S_a) to original cross-section area (S) for a core.[54]

Damage variable F is given by mathematical eq 33

$$F = \frac{S_a}{S} = \frac{x \cdot D}{L \cdot D} \tag{33}$$

where x is the water penetration depth into the matrix, m, and D is the diameter of the core, m.

The cross-section area for the unaltered zone is transformed according to eq 33

$$S_{ua} = S(1 - F) \tag{34}$$

where S_{ua} is the cross-section area, m^2.

Assumed that the external load (F) is a constant during loading, we can state that during the prefailure period, there exists[55]

$$F{=}\sigma S = \sigma_{ua} S_{ua} \tag{35}$$

where σ and σ_{ua} are the load stress prior to and post-treatment, Pa.

Based on the theory of damage mechanics, the constitutive relation for the core before the water uptake process and post-imbibition takes the form of eqs 36 and 37[56]

$$\sigma{=}E\varepsilon \tag{36}$$

$$\sigma_{ua} = E_{ua}\varepsilon \tag{37}$$

where E and E_{ua} are the Young's elastic modulus prior to and post-treatment, Pa, and ε is the strain that corresponds to the stress, m.

Combing 35, 36, and 37, the elastic modulus of altered core in the core can be derived, as seen in eq 38

$$E_{ua} = E(1 - F) \tag{38}$$

3.4.2. Shale Compressibility Model. The pore compressibility has a close relationship with different types of rocks and pore shape. For example, the compressibility for circular pore model has been put forward, given by eq 39[57]

$$C_p = \frac{2(1+v)}{E} \tag{39}$$

where v is the Poisson's ratio, dimensionless.

The value of Poisson's ratio has a weak influence on pore compressibility. Hence, for circular pore geometries, pore compressibility depends on the magnitude of Young's modulus.[58]

3.4.3. Permeability Model with Stress Sensitivity. Due to its form simplicity, an exponential function[59] is frequently adopted to describe the stress-dependent permeability of tight formations, as expressed in eq 40

$$K_m = K e^{-\gamma(p-p_p)} \tag{40}$$

where K_m is the permeability considering stress sensitivity, m^2; y is the stress sensitivity coefficient, denoting the severity of formation stress sensitivity, Pa^{-1}; and p_p is the pore pressure, Pa.

https://doi.org/10.1021/acsomega.3c06079
ACS Omega 2023, 8, 46746−46756

It is proved that the stress-sensitive coefficient is the product of porosity sensitivity exponent α and the pore compressibility C_p, which is given by eq 41[60]

$$\gamma = \alpha C_p \tag{41}$$

It is demonstrated that long-term fracturing fluid soaking can cause irreversible damage to mechanical properties, including Young's modulus and the uniaxial compression strength.[61] We can conclude from Figure 20 that long-term water soaking with

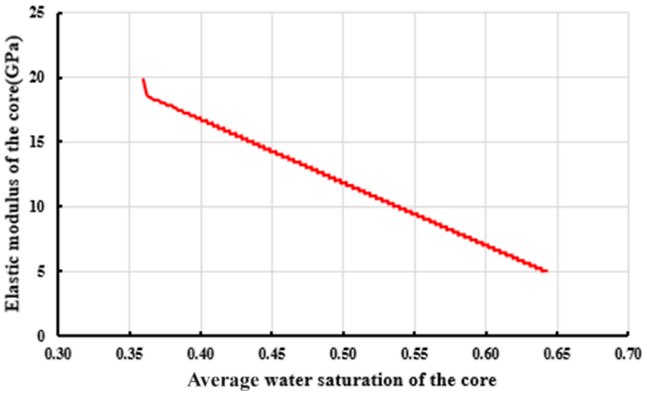

Figure 20. Elastic modulus versus the average saturation curve at the core-scale.

the core can induce the reduction in the rock elastic modulus, caused by weakening of the joint strength between mineral particles and further destroying the original shale structure. It further leads to the significant increase in the compressive strength, as seen from Figure 21. Meanwhile, it is testified that the rock−water interaction can make it possible to reduce rock stress sensitivity, as given by eq 41.

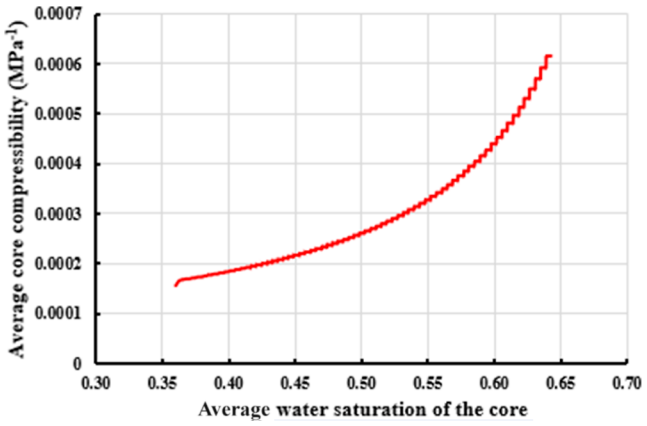

Figure 21. Compressibility strength versus the average saturation curve at the core-scale.

Figure 22 depicts a comparison of the shale permeability change with alteration in net pore pressure. As seen in Figure 22, the permeability drops rapidly with respect to the increasing net pore pressure in the case of the water imbibition effect. Without water imbibition, the permeability declines relatively slightly when the net pore pressure increases, indicating that the water invasion process can enhance formation stress sensitivity and further have a large impact in gas flow. It is observed as well in Figure 22 that the more driving forces are considered in the model, the more water

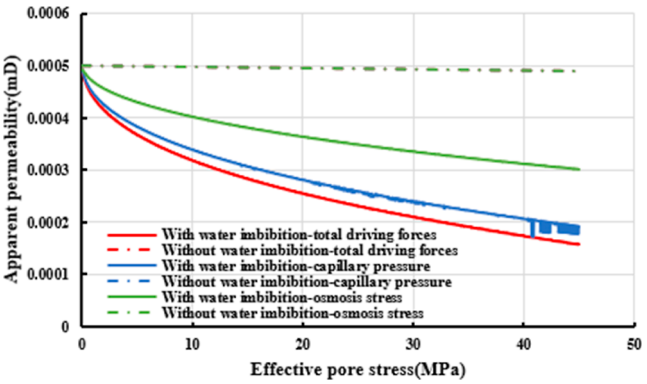

Figure 22. Compressibility strength versus the average saturation curve at the core-scale.

enters into the micropores and, thus, the more stress sensitive the core might be. It is because the apparent permeability with the impact of total forces decreases most significantly compared to other two cases with the water imbibition process.

4. CONCLUSIONS

In this study, we set up a one-dimensional water uptake model based on the unsaturated flow theory with the different sets of driving mechanisms taken into account. This model investigates water imbibition into the shale matrix and furthermore clarifies water distribution in shales at different shut-in periods. The quantitative correlation of the water uptake process and petrophysical alteration was predicted as well.

The following main conclusions can be drawn:

(1) The water imbibition process is assumed to be driven by both capillary pressure and chemical osmosis effect, which is incorporated in the numerical model. The model was validated to be reliable based on the history-fitting results between experimental results and mathematical simulations. Moreover, more water can occupy shale micropores compared to that dominated by only one kind of driving force. This model is used to predict and compare water penetration and its effects on the reservoir properties.

(2) The water penetration profiles were obtained using the imbibition model. In case of total driving forces, it takes 14 days for fracture fluid to move forward into the matrices at over one-half in core length. However, the thickness of altered zone is less than one-10th in core length controlled by capillary and osmosis. As a result, the capillary pressure plays a more crucial part in the total driving forces than osmosis pressure.

(3) Last but not at least, we plotted the shale porosity and permeability curves at different shut-in periods and different driving mechanisms. The core altered zone has a relatively lower permeability than that of original core. The permeability and porosity both increase significantly at the early stage but slightly at the later stage. The more driving forces will induce more water invasion into the matrix and promote water front to move farther into the media, leading to a gradual increase in the water intrusion depth. Furthermore, we determined the correlation between core permeability, porosity, and average water saturation. We found that both porosity and permeability are negatively associated with water saturation, which is supported by publications.[33,34]

https://doi.org/10.1021/acsomega.3c06079
ACS Omega 2023, 8, 46746−46756

(4) Finally, we determined the shale mechanical alteration caused by water uptake process, such as elastic modulus and compressive strength, and further compared shale apparent permeability response with net pore pressure change prior to and post water imbibition, respectively. Long-term water soaking can result in rock softening by mainly destroying the shale original microstructure and weakening the joint strength between water-sensitive particles. It ultimately leads to a significant reduction in the elastic modulus, but an increase in the shale compressive strength and stress sensitivity. As a result, shale apparent permeability will drop more rapidly under the net pore pressure after water imbibition compared to that without a water uptake.

The numerical model developed in this study will provide efficient insights into water imbibition driving mechanisms for unconventional hydrocarbon reservoir systems. It is important for better understanding of shale alteration due to the HFF-rock interaction, which is useful for predicting long-term hydrocarbon production from shale reservoirs.

■ ASSOCIATED CONTENT

Data Availability Statement

The data that support the findings of this study are not available for now due to the ongoing project. Otherwise, it can be accessible from the corresponding author upon reasonable request.

■ AUTHOR INFORMATION

Corresponding Author

Yingying Xu − *University of the Chinese Academy of Sciences, Beijing 100049, China; Institute of Porous Flow and Fluid Mechanics, Chinese Academy of Sciences, Langfang 065007, China; Research Institute of Petroleum Exploration and Development, PetroChina, Beijing 100083, China;* orcid.org/0000-0001-8224-2342; Email: xuyingying01@pertrochina.com.cn

Authors

Hai Li − *PetroChina Southwest Oil and Gas Field Company Exploration and Development Research Institute, Chengdu, Sichuan 610000, China*

Zhiming Hu − *Research Institute of Petroleum Exploration and Development, PetroChina, Beijing 100083, China*

Xiangui Liu − *Research Institute of Petroleum Exploration and Development, PetroChina, Beijing 100083, China*

Xianggang Duan − *Research Institute of Petroleum Exploration and Development, PetroChina, Beijing 100083, China*

Jin Chang − *Research Institute of Petroleum Exploration and Development, PetroChina, Beijing 100083, China*

Complete contact information is available at: https://pubs.acs.org/10.1021/acsomega.3c06079

Notes

The authors declare no competing financial interest.

■ ACKNOWLEDGMENTS

This research was funded by the Research on New Techniques and Methods of Shale Gas Experimental Testing (grant no. 2021DJ1905).

■ REFERENCES

(1) Tokunaga, T. K.; Shen, W.; Wan, J.; Kim, Y.; Cihan, A.; Zhang, Y.; Finsterle, S. Water saturation relations and their diffusion-limited equilibration in gas shale: Implications for gas flow in unconventional reservoirs. *Water Resour. Res.* **2017**, *53* (11), 9757−9770.

(2) King, G. E. Hydraulic fracturing 101: What every representative, environmentalist, regulator, reporter, investor, university researcher, neighbor and engineer should know about estimating frac risk and improving frac performance in unconventional gas and oil wells. In *SPE Hydraulic Fracturing Technology Conference and Exhibition*; OnePetro, 2012;.

(3) Roychaudhuri, B.; Tsotsis, T.; Jessen, K. An experimental investigation of spontaneous imbibition in gas shales. *J. Pet. Sci. Eng.* **2013**, *111*, 87−97.

(4) Singh, H. A critical review of water uptake by shales. *J. Nat. Gas Sci. Eng.* **2016**, *34*, 751−766.

(5) Fan, L.; et al. Understanding gas production mechanism and effectiveness of well stimulation in the Haynesville Shale through reservoir simulation. In *Canadian Unconventional Resources and International Petroleum Conference*; OnePetro, 2010;.

(6) Morrow, N. R.; Mason, G. Recovery of oil by spontaneous imbibition. *Curr. Opin. Colloid Interface Sci.* **2001**, *6* (4), 321−337.

(7) Unsal, E.; Mason, G.; Morrow, N.; Ruth, D. Co-current and counter-current imbibition in independent tubes of non-axisymmetric geometry. *J. Colloid Interface Sci.* **2007**, *306* (1), 105−117.

(8) Lyu, C.; Ning, Z.; Chen, M.; Wang, Q. Experimental study of boundary condition effects on spontaneous imbibition in tight sandstones. *Fuel* **2019**, *235*, 374−383.

(9) Cheng, Z.; Wang, Q.; Ning, Z.; Li, M.; Lyu, C.; Huang, L.; Wu, X. Experimental investigation of countercurrent spontaneous imbibition in tight sandstone using nuclear magnetic resonance. *Energy Fuels* **2018**, *32* (6), 6507−6517.

(10) Pagels, M.; et al. Quantifying fracturing fluid damage on reservoir rock to optimize production. In *SPE/AAPG/SEG Unconventional Resources Technology Conference*; OnePetro, 2013;.

(11) Bertoncello, A.; Wallace, J.; Blyton, C.; Honarpour, M.; Kabir, C. S. Imbibition and water blockage in unconventional reservoirs: well-management implications during flowback and early production. *SPE Reservoir Eval. Eng.* **2014**, *17* (04), 497−506.

(12) Bostrom, N.; et al. The time-dependent permeability damage caused by fracture fluid. In *SPE International Symposium and Exhibition on Formation Damage Control*; OnePetro, 2014;.

(13) Cai, J.; Yu, B. A discussion of the effect of tortuosity on the capillary imbibition in porous media. *Transp. Porous Media* **2011**, *89* (2), 251−263.

(14) Mason, G.; Morrow, N. R. Developments in spontaneous imbibition and possibilities for future work. *J. Pet. Sci. Eng.* **2013**, *110*, 268−293.

(15) Yang, F.; Lyu, B.; Xu, S. Water sorption and transport in shales: an experimental and simulation study. *Water Resour. Res.* **2021**, *57* (2), No. e2019WR026888.

(16) Zhou, Z.; Abass, H.; Li, X.; Bearinger, D.; Frank, W. Mechanisms of imbibition during hydraulic fracturing in shale formations. *J. Pet. Sci. Eng.* **2016**, *141*, 125−132.

(17) Binazadeh, M.; et al. Effect of electrostatic interactions on water uptake of gas shales: the interplay of solution ionic strength and electrostatic double layer. *Energy Fuels* **2016**, *30* (2), 992−1001.

(18) Dehghanpour, H.; Zubair, H. A.; Chhabra, A.; Ullah, A. Liquid intake of organic shales. *Energy Fuels* **2012**, *26* (9), 5750−5758.

(19) Ge, H. K.; Yang, L.; Shen, Y. H.; Ren, K.; Meng, F. B.; Ji, W. M.; Wu, S. Experimental investigation of shale imbibition capacity and the factors influencing loss of hydraulic fracturing fluids. *Pet. Sci.* **2015**, *12* (4), 636−650.

(20) Li, X. et al. The impact of water salinity/surfactant on spontaneous imbibition through capillarity and osmosis for unconventional IOR. In *SPE/AAPG/SEG Unconventional Resources Technology Conference*; OnePetro, 2016

(21) Marine, I. W.; Fritz, S. J. Osmotic model to explain anomalous hydraulic heads. *Water Resour. Res.* **1981**, *17* (1), 73−82.

https://doi.org/10.1021/acsomega.3c06079
ACS Omega 2023, 8, 46746−46756

(22) Yang, L.; Ge, H.; Shi, X.; Li, J.; Zhou, T.; Cao, W.; Zhang, K.; Zhang, Y.; Gao, M. Experimental and numerical study on the relationship between water imbibition and salt ion diffusion in fractured shale reservoirs. *J. Nat. Gas Sci. Eng.* **2017**, *38*, 283−297.
(23) (a) Lomba, E. F. T.; Chenevert, M. E.; Sharma, M. M. The role of osmotic effects in fluid flow through shales. *J. Pet. Sci. Eng.* **2000**, *25* (1), 25−35. (b) Lomba, R. F.; et al. The role of osmotic effects in fluid flow through shales. *J. Pet. Sci. Eng.* **2000**, *25* (1−2), 25−35.
(24) Rahman, M. M.; Chen, Z.; Rahman, S. S. Experimental investigation of shale membrane behavior under tri-axial condition. *Pet. Sci. Technol.* **2005**, *23* (9−10), 1265−1282.
(25) Cheng, J.; Wan, Z.; Zhang, Y.; Li, W.; Peng, S. S.; Zhang, P. Experimental study on anisotropic strength and deformation behavior of a coal measure shale under room dried and water saturated conditions. *Shock Vib.* **2015**, *2015*, 1−13.
(26) Al-bazali, T. A novel experimental technique to monitor the time-dependent water and ions uptake when shale interacts with aqueous solutions. *Rock Mech.* **2013**, *46* (5), 1145−1156.
(27) Wong, R. C. K. Swelling and softening behaviour of La Biche shale. *Can. Geotech. J.* **1998**, *35* (2), 206−221.
(28) Liu, K.; Sheng, J. J. A new experimental methodology to investigate water adsorption into shale under stress anisotropy conditions. In *SPE Liquids-Rich Basins Conference - North America*; OnePetro, 2019
(29) Shen, Y.; Ge, H.; Meng, M.; Jiang, Z.; Yang, X. Effect of water imbibition on shale permeability and its influence on gas production. *Energy Fuels* **2017**, *31* (5), 4973−4980.
(30) Wang, Q.; Lyu, C.; Cole, D. R. Effects of hydration on fractures and shale permeability under different confining pressures: An experimental study. *J. Pet. Sci. Eng.* **2019**, *176*, 745−753.
(31) Roshan, H.; Ehsani, S.; Marjo, C.; Andersen, M.; Acworth, R. Mechanisms of water adsorption into partially saturated fractured shales: An experimental study. *Fuel* **2015**, *159*, 628−637.
(32) Tangparitkul, S.; Saul, A.; Leelasukseree, C.; Yusuf, M.; Kalantariasl, A. Fines migration and permeability decline during reservoir depletion coupled with clay swelling due to low-salinity water injection: An analytical study. *J. Pet. Sci. Eng.* **2020**, *194*, 107448.
(33) Aksu, I.; Bazilevskaya, E.; Karpyn, Z. Swelling of clay minerals in unconsolidated porous media and its impact on permeability. *GeoResJ.* **2015**, *7*, 1−13.
(34) Chenevert, M. E. Shale alteration by water adsorption. *J. Pet. Technol.* **1970**, *22* (09), 1141−1148.
(35) Bostrom, N.; et al. The time-dependent permeability damage caused by fracture fluid. In *SPE International Symposium and Exhibition on Formation Damage Control*; OnePetro, 2014
(36) Bai, J.; Kang, Y.; Chen, M.; Li, X.; You, L.; Chen, Z.; Fang, D. Impact of water film on methane surface diffusion in gas shale organic nanopores. *J. Pet. Sci. Eng.* **2021a**, *196*, 108045.
(37) Bai, J.; Kang, Y.; Chen, M.; Chen, Z.; You, L. Impact of the Water Adsorption Monolayer on Methane Ad-/Desorption Behavior in Gas Shale Nanopores. *Ind. Eng. Chem. Res.* **2021b**, *60* (7), 3130−3141.
(38) Chen, M.; Bai, J.; Kang, Y.; Chen, Z.; You, L.; Li, X.; Liu, J.; Zhang, Y. Redistribution of fracturing fluid in shales and its impact on gas transport capacity. *J. Nat. Gas Sci. Eng.* **2021**, *86*, 103747.
(39) Yang, F.; Zheng, H.; Guo, Q.; Lyu, B.; Nie, S.; Wang, H. Modeling Water Imbibition and Penetration in Shales: New Insights into the Retention of Fracturing Fluids. *Energy Fuels* **2021**, *35* (17), 13776−13787.
(40) Yang, L.; Ge, H.; Shi, X.; Li, J.; Zhou, T.; Cao, W.; Zhang, K.; Zhang, Y.; Gao, M. Experimental and numerical study on the relationship between water imbibition and salt ion diffusion in fractured shale reservoirs. *J. Nat. Gas Sci. Eng.* **2017**, *38*, 283−297.
(41) Li, X. et al. A shale matrix imbibition model−interplay between capillary pressure and osmotic pressure. In *SPE Annual Technical Conference and Exhibition*; OnePetro, 2016
(42) Zan, Y.; Yu, Q. Experimental investigation of spontaneous water imbibition into methane-saturated shales under different methane pressures. *Energy Fuels* **2020**, *34* (11), 14356−14367.
(43) Zhang, R. et al. A fully coupled model of non-isothermal multiphase flow, geomechanics, and chemistry during CO2 sequestration in brine aquifers. In *Proceeding TOUGH. Symposium*, 2012; pp 838−848.
(44) Zhang, R. et al. A fully coupled model of non-isothermal multiphase flow, solute transport and reactive chemistry in porous media. In *SPE Annual Technical Conference and Exhibition*; OnePetro, 2012
(45) Al-Bazali et al. Factors controlling the membrane efficiency of shales when interacting with water-based and oil-based muds. In *International Oil & Gas Conference and Exhibition in China*; OnePetro, 2006
(46) Qiao, C.; Li, L.; Johns, R. T.; Xu, J. A mechanistic model for wettability alteration by chemically tuned waterflooding in carbonate reservoirs. *SPE J.* **2015**, *20* (04), 767−783.
(47) Zhang, R.; Winterfeld, P. H.; Yin, X.; Xiong, Y.; Wu, Y. S. Sequentially coupled THMC model for CO2 geological sequestration into a 2D heterogeneous saline aquifer. *J. Nat. Gas Sci. Eng.* **2015**, *27*, 579−615.
(48) Standnes, D. C.; Andersen, P. Ø.; Papatzacos, P.; Skjæveland, S. M. Interpretation of 1-D Counter-Current Spontaneous Imbibition Processes Using Microscopic Diffusion Theory and a Modified Buckley−Leverett Approach. *Energy Fuels* **2020**, *34* (5), 5868−5883.
(49) Shen, Y.; Ge, H.; Meng, M.; Jiang, Z.; Yang, X. Effect of water imbibition on shale permeability and its influence on gas production. *Energy Fuels* **2017**, *31* (5), 4973−4980.
(50) Brooks, R. H.; Corey, A. T. Properties of porous media affecting fluid flow. *J. Irrig. Drain. Div., Am. Soc. Civ. Eng.* **1966**, *92* (2), 61−88.
(51) Engelder, T.; Cathles, L. M.; Bryndzia, L. T. The fate of residual treatment water in gas shale. *J. Unconv. Oil Gas Resour.* **2014**, *7*, 33−48.
(52) Xu, Y.; Xiang, G.; Jiang, H.; Chen, T.; Chu, F. Role of osmotic suction in volume change of clays in salt solution. *Appl. Clay Sci.* **2014**, *101*, 354−361.
(53) Bear, J. *Dynamics of fluids in porous media*; Courier Corporation, 1988.
(54) Zhu, W. C.; Wei, C. H. Numerical simulation on mining-induced water inrushes related to geologic structures using a damage-based hydromechanical model. *Environ. Earth Sci.* **2011**, *62* (1), 43−54.
(55) Tang, C. A.; Tham, L.; Lee, P.; Yang, T.; Li, L. Coupled analysis of flow, stress and damage (FSD) in rock failure. *Int. J. Rock Mech. Min. Sci.* **2002**, *39* (4), 477−489.
(56) Guo, J.; Zeng, F.; Zhao, J. A model for predicting reservoir fracturing pressure of perforated wells after acid damage. *Adv. Pet. Explor. Dev.* **2011**, *38* (2), 221−227.
(57) Al-Wardy, W.; Zimmerman, R. W. Effective stress law for the permeability of clay-rich sandstones. *J. Geophys. Res.: Solid Earth* **2004**, *109*, B04203, DOI: 10.1029/2003jb002836.
(58) Zhang, R.; Ning, Z.; Yang, F.; Wang, X.; Zhao, H.; Wang, Q. Impacts of nanopore structure and elastic properties on stress-dependent permeability of gas shales. *J. Nat. Gas Sci. Eng.* **2015**, *26*, 1663−1672.
(59) McKee, C. R.; Bumb, A. C.; Koenig, R. A. Stress-dependent permeability and porosity of coal and other geologic formations. *SPE Form. Eval.* **1988**, *3* (01), 81−91.
(60) David, C.; Wong, T. F.; Zhu, W.; Zhang, J. Laboratory measurement of compaction-induced permeability change in porous rocks: Implications for the generation and maintenance of pore pressure excess in the crust. *Pure Appl. Geophys.* **1994**, *143* (1−3), 425−456.
(61) Zhang, J.; Kamenov, A.; Zhu, D.; Hill, A. Development of new testing procedures to measure propped fracture conductivity considering water damage in clay-rich shale reservoirs: An example of the Barnett Shale. *J. Pet. Sci. Eng.* **2015**, *135*, 352−359.

https://doi.org/10.1021/acsomega.3c06079
ACS Omega 2023, 8, 46746−46756